

Airborne laser scanning and tree crown fragmentation metrics for the assessment of *Phytophthora ramorum* infected larch forest stands



Chloe Barnes^{a,*}, Heiko Balzter^{a,b}, Kirsten Barrett^a, James Eddy^c, Sam Milner^d, Juan C. Suárez^e

^a University of Leicester, Leicester Institute for Space and Earth Observation (LISEO), Centre for Landscape and Climate Research, Department of Geography, University Road, Leicester LE1 7RH, UK

^b NERC National Centre for Earth Observation (NCEO) at University of Leicester, University Road, Leicester LE1 7RH, UK

^c Bluesky International Limited, The Old Toy Factory, Jackson Street, Coalville, Leicestershire LE67 3NR, UK

^d Natural Resources Wales, Clawdd Newydd, Ruthin, Denbighshire LL14 2NL, UK

^e Forest Research, Northern Research Station, Roslin, Midlothian EH25 9SY, UK

ARTICLE INFO

Keywords:

Phytophthora ramorum

Larch

LiDAR

Tree disease

ABSTRACT

The invasive phytopathogen *Phytophthora ramorum* has caused extensive infection of larch forest across areas of the UK, particularly in Southwest England, South Wales and Southwest Scotland. At present, landscape level assessment of the disease in these areas is conducted manually by tree health surveyors during helicopter surveys. Airborne laser scanning (ALS), also known as LiDAR, has previously been applied to the segmentation of larch tree crowns infected by *P. ramorum* infection and the detection of insect pests in coniferous tree species. This study evaluates metrics from high-density discrete ALS point clouds (24 points/m²) and canopy height models (CHMs) to identify individual trees infected with *P. ramorum* and to discriminate between four disease severity categories (NI: not infected, 1: light, 2: moderate, 3: heavy). The metrics derived from ALS point clouds include canopy cover, skewness, and bintiles (B60, B70, B80 and B90) calculated using both a static (1 m) and a variable (50% of tree height) cut-off height. Significant differences are found between all disease severity categories, except in the case of healthy individuals (NI) and those in the early stages of infection (category 1). In addition, fragmentation metrics are shown to identify the increased patchiness and intra-crown height irregularities of CHMs associated with individual trees subject to heavy infection (category 3) of *P. ramorum*. Classifications using a k-nearest neighbour (k-NN) classifier and ALS point cloud metrics to classify disease presence/absence and severity yielded overall accuracies of 72% and 65% respectively. The results indicate that ALS can be used to identify individual tree crowns subject to moderate and heavy *P. ramorum* infection in larch forests. This information demonstrates the potential applications of ALS for the development of a targeted phytosanitary approach for the management of *P. ramorum*.

1. Introduction

UK forestry has experienced notable introductions of several significant phytopathogens in recent decades (Brown et al., 2003; Brasier, 2008; Webber et al., 2008; Mitchell et al., 2014). Subsequent to its identification in the UK in 2002 (Lane et al., 2003), *Phytophthora ramorum* has caused extensive infection of larch (*Larix* sp.) trees, particularly across forests situated in Southwest England, South Wales and Southwest Scotland (Forestry Commission, 2016). The infection which can present both stem and foliar symptoms in affected larch, such as stem bleeds, foliage discolouration and defoliation (Webber et al., 2010) has resulted in the felling of over 16,000 ha of larch across the UK, including Japanese (*Larix kaempferi*), European (*Larix decidua*) and

hybrid species (*Larix x eurolepis*) (Forestry Commission, 2014).

Current efforts to assess landscape-level patterns of *P. ramorum* infection and identify new outbreaks rely on visual aerial assessment conducted by tree-health surveyors during helicopter surveys. In this instance, foliar symptoms presented by infected larch aid the identification of *P. ramorum*. The use of manual aerial detection highlights an opportunity for the application of remote sensing to detect and assess *P. ramorum* outbreaks in larch stands (Medcalf et al., 2011). Despite the increased recognition of remote sensing as a tool for the assessment of forest health and disease, visual surveys continue to dominate in the operational management of pests and phytopathogens in the forestry sector (Hall et al., 2016; Lausch et al., 2017). Commonly cited concerns and barriers to the application of remote sensing techniques for the

* Corresponding author.

E-mail addresses: cb482@le.ac.uk (C. Barnes), hb91@le.ac.uk (H. Balzter), kb308@le.ac.uk (K. Barrett), james.eddy@bluesky-world.com (J. Eddy), Sam.Milner@cyfoethnaturiolcymru.gov.uk (S. Milner), juan.suarez@forestry.gsi.gov.uk (J.C. Suárez).

<http://dx.doi.org/10.1016/j.foreco.2017.08.052>

Received 15 June 2017; Received in revised form 29 August 2017; Accepted 31 August 2017

Available online 09 September 2017

0378-1127/ Crown Copyright © 2017 Published by Elsevier B.V. This is an open access article under the OGL license (<http://creativecommons.org/licenses/OGL/3.0/>).

assessment of forest condition include the perceived insufficient resolution associated with optical satellite data and the costs associated with data acquisition and processing (Suárez et al., 2005; Rullan-Silva et al., 2013; Hall et al., 2016). Recognising the concerns of end-users is important for implementation of the results from scientific research into forestry management practise (Wulder et al., 2006).

In forest research, remote sensing methodologies utilising airborne laser scanning (ALS), also known as airborne light detection and ranging (LiDAR), have been extensively applied to provide information regarding the structural character of vegetation in these landscapes (Lim et al., 2003; Wulder et al., 2013; Sheridan et al., 2015). ALS provides three-dimensional data that have previously been employed to examine biophysical forest parameters (Zimble et al., 2003; Balzter et al., 2007; Yoga et al., 2017). In addition, ALS datasets facilitate the segmentation of individual tree crowns (ITCs) (Brandtberg et al., 2003; Barnes et al., 2017), which can subsequently be applied to determine ITC-based metrics such as tree height, crown diameter, canopy cover and species (Popescu et al., 2003; Holmgren and Persson, 2004; Reutebuch et al., 2005; Breidenbach et al., 2010).

One application of ALS for the assessment of crown condition utilises parameters derived from point clouds to assess the three-dimensional structure of trees and their canopies (Kwak et al., 2010). Previous studies have used height related metrics from ALS point clouds to characterise tree structure and identify crown decline for an array of applications including habitat suitability mapping (Martinuzzi et al., 2009; Casas et al., 2016) and the assessment of insect pest outbreaks (Bright et al., 2013; Vastaranta et al., 2013). These metrics can be categorised into three broad categories: height-based metrics and percentiles, distributional metrics and cover metrics. Height-based metrics and percentiles summarise patterns regarding the height of ALS returns. Distributional metrics concern the distribution of returns through the canopy profile, whilst cover metrics typically compare two subsets of points to produce a variety of indices. (Coops et al., 2009). In addition, ALS point cloud intensity characteristics, which concern the strength of pulse backscattering, have also been applied to the assessment of crown decline, largely with regards to the identification of dead trees (Kim et al., 2009; Wing et al., 2015; Casas et al., 2016).

In the specific context of disease outbreaks in forestry, a series of height related ALS-metrics including the number of canopy returns, maximum height, standard deviation of height, percentage of returns below 10%, 50%, 80% and 90% of total height and gap fraction have all previously been applied to the assessment of defoliation from insect pests (Solberg et al., 2006; Coops et al., 2009; Kantola et al., 2010; Vastaranta et al., 2013). In particular, Kantola et al. (2010) and Vastaranta et al. (2013) reported accuracies of 80.7% and 84.3% for the respective tree- and plot-level classifications of healthy and defoliated Scots pine (*Pinus sylvestris*) affected by the common pine sawfly (*Diprion pini*). The success of ALS height metrics for the assessment of insect pest defoliation can be attributed to the increased penetration of laser pulses into the forest canopy when foliage is lost (Coops et al., 2009; Kantola et al., 2010; Vastaranta et al., 2013). Nevertheless, the potential use of these ALS-derived metrics has not previously been considered for disease outbreaks resulting from phytopathogens such as *P. ramorum*.

In addition to the three-dimensional analysis of ALS point clouds, the impacts of dieback and defoliation of tree crowns are also evident in ALS-derived canopy height models (CHMs) as increased irregularities in surface elevation across individual crowns (Holdenrieder et al., 2004). CHMs are a common raster product derived from ALS datasets to represent the canopy surface, typically computed via the subtraction of the digital terrain model (DTM) and digital surface model (DSM) which represent the rasterised last and first returns respectively (Dubayah and Drake, 2000; Ben-Arie et al., 2009). As a result of increased penetration of ALS pulses through defoliated canopies, crowns subject to disease typically exhibit a patchy appearance when viewed as CHMs (Holdenrieder et al., 2004; Barnes et al., 2017). Landscape metrics traditionally applied to assess habitat fragmentation in the field of

landscape ecology provide a means of quantifying the characteristics and spatial distribution of patches (Hargis et al., 1998; Kupfer, 2012). This study applies this series of metrics to assess the increased patchiness of CHMs for ITCs subject to disease.

Relationships between remotely sensed and ground-based metrics facilitate classifications of tree crown condition, providing a spatial representation of disease or decline throughout forested environments and hence a useful tool for disease management (Shendryk et al., 2016). The selection of disease severity category boundaries is particularly important, with difficulties previously noted in the differentiation between classes across the spectrum of moderate disease severity for forest pests (Coops et al., 2003; Leckie et al., 2005). A range of established classifiers including k-nearest neighbour (k-NN) and random forest (RF) have previously been applied to the classification of disease and vegetation structure (McInerney and Nieuwenhuis, 2009; Kantola et al., 2010; Bright et al., 2013; Ortiz et al., 2013), each presenting advantages and limitations, with suitability largely dependent on input data characteristics such as the quantity of training data and class separability (Huang et al., 2002; Samaniego et al., 2008).

This study uses ALS in the form of point cloud metrics and fragmentation metrics from CHMs to identify individual tree crowns subject to *P. ramorum* infection and examine the capability of these metrics to provide separation of four disease severity classes (NI: not infected, 1: light, 2: moderate, 3: heavy) based on differences in tree crown structure. Furthermore, the application of ALS metrics for the classification of *P. ramorum* presence and disease severity were also evaluated with the use of the k-NN and RF classifiers.

2. Material and methods

2.1. Study area

The study was conducted in Wales, United Kingdom. The two study areas were situated at Ogmores Forest in South Wales (51.5954°N, –3.5320°W) and Radnor Forest in Mid Wales (52.2708°N, –3.1503°W) (Fig. 1), both managed by Natural Resources Wales. Ogmores Forest is situated within the core *P. ramorum* disease zone in Wales and has been subject to the infection since 2011. Due to the spread of the *P. ramorum* across the Ogmores site, a second site, Radnor Forest, comprising of healthy larch stands was selected outside of the core *P. ramorum* zone. To aid accessibility for ground surveying, a combination of plots and transects were established along sub-compartment edges. Table 1 provides a summary of the sample transects from both study sites, variation in transect lengths was incurred due to differences in sub-compartment dimensions. A total of 258 trees were surveyed, with 158 and 100 individuals from the Ogmores and Radnor Forests respectively. Test and training datasets were subsequently identified by dividing each sample plot in half.

2.2. Field data collection

Trees located within selected sampling areas at both study sites were individually tagged, photographed and surveyed for species and diameter breast height. The position of each individual was recorded using a handheld Garmin Oregon 550t GPS. In circumstances of poor GPS positional accuracy (> 2 m), the distance and bearing of individuals was also noted from a reference point situated outside the forest. Larch species, which formed the majority of surveyed individuals (84%) were subject to additional visual surveying of both the stem and crown to ascertain the overall tree health and the occurrence and severity of *P. ramorum* infection. The presence or absence of cankers, bark stripping and foliage colour change were noted, as well as percentage classes (10% intervals) of deadwood, defoliation, discolouration, wilting and canopy cover. Visual assessments were conducted by the same surveyor throughout the data collection to ensure consistency (Kantola et al., 2010; Nutter et al., 2010). Surveys were conducted in

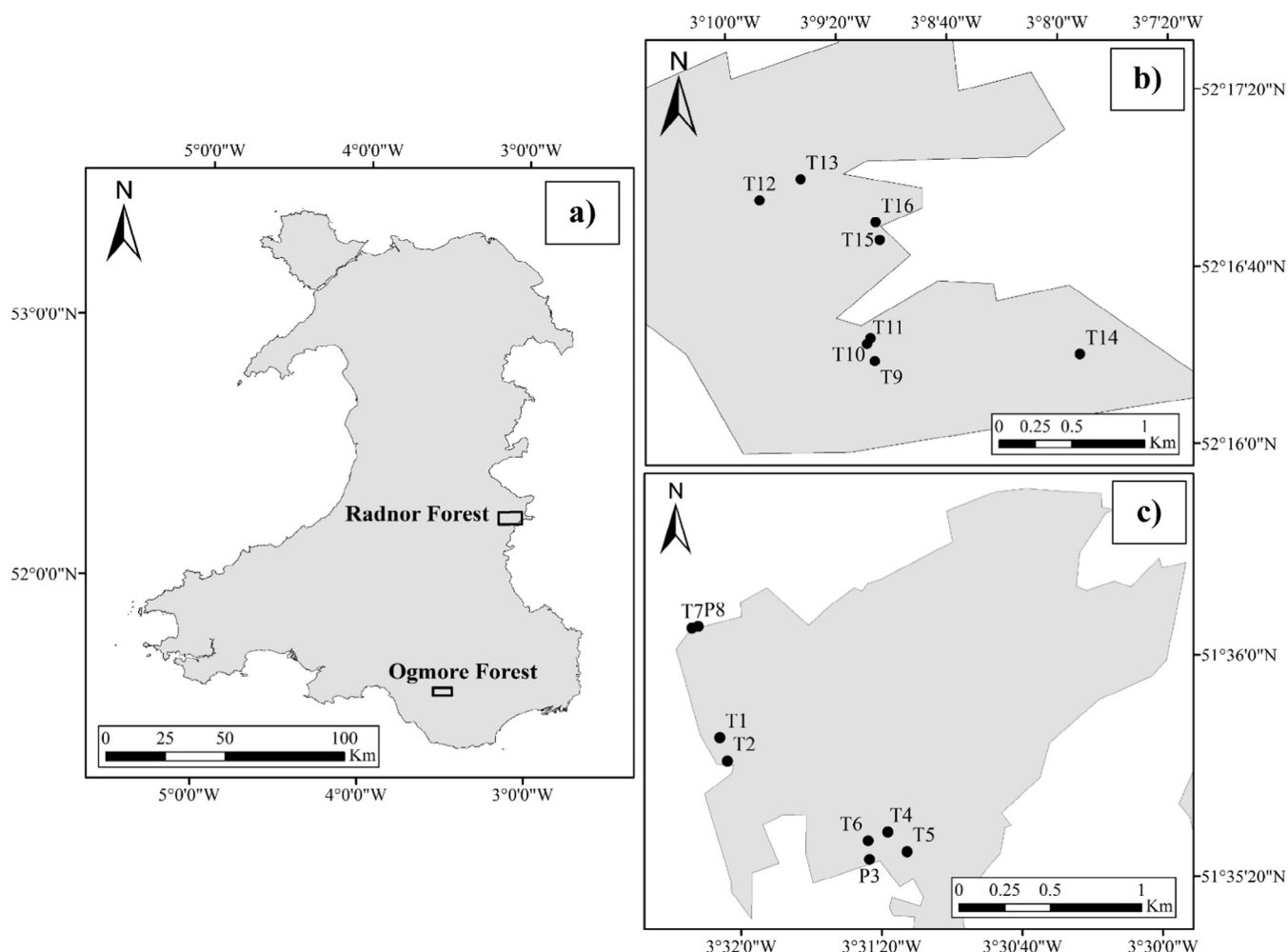


Fig. 1. (a) Location of study areas in Wales; (b) Location of transects at the Radnor site, grey indicates forested area; (c) Location of transects and plots at the Ogmores site, grey indicates forested area.

June, July and August 2015 coinciding with the acquisition of ALS data for both study sites by Bluesky International. At the infected study site, larch trees which exhibited characteristic cankers associated with *P. ramorum* were presumed infected. In circumstances where the presence of *P. ramorum* infection was not definitive from presented symptoms, a

lateral flow device (LFD) was used to ascertain the presence of *Phytophthora spp.* in suspect plant material (Kox et al., 2007). A total of three LFD tests were undertaken before a tree was classified as not infected, in order to reduce false negatives.

To evaluate the severity of *P. ramorum* infections the scoring system

Table 1

Characteristics of the sample transects and plots established at the Ogmores and Radnor Forests. Tree heights have been calculated using the ALS data (June 2015) and the size, number of trees and *P. ramorum* presence were recorded during field surveys (June, July and August 2015).

No.	Forest	Species Composition	Max Height (m)	Min Height (m)	Mean Height (m)	Transect Length (m) ^a / Plot Size (m ²) ^b	No. Trees	<i>P. ramorum</i> Infection confirmed	Percentage of Larch Trees with <i>P. ramorum</i> Infection (%)
T1	Ogmores	HL, MB	8.41	4.03	6.01	100 ^a	22	Yes	44
T2	Ogmores	HL, MB	11.54	4.98	8.82	100 ^a	24	Yes	75
P3	Ogmores	JL	18.84	10.90	16.44	900 ^b	22	Yes	75
T4	Ogmores	JL, SS	14.48	6.87	10.00	130 ^a	30	Yes	95
T5	Ogmores	JL	16.64	9.09	13.80	30 ^a	5	Yes	100
T6	Ogmores	JL	20.30	10.18	15.82	130 ^a	9	Yes	100
T7	Ogmores	JL	21.52	11.90	18.87	50 ^a	10	Yes	100
P8	Ogmores	JL	24.59	15.55	21.73	1000 ^b	36	Yes	100
T9	Radnor	JL, MB	21.19	14.61	19.15	60 ^a	11	No	N/A
T10	Radnor	HL, MB, MC	6.88	4.69	5.44	60 ^a	15	No	N/A
T11	Radnor	JL, MB	19.58	13.14	15.65	60 ^a	20	No	N/A
T12	Radnor	JL	32.78	22.69	29.33	60 ^a	7	No	N/A
T13	Radnor	EL, HL	33.04	26.95	30.46	100 ^a	12	No	N/A
T14	Radnor	SS	25.49	21.09	23.84	60 ^a	5	No	N/A
T15	Radnor	JL	18.15	14.67	16.34	100 ^a	9	No	N/A
T16	Radnor	JL	26.79	11.67	21.21	100 ^a	21	No	N/A

Abbreviations: EL, European Larch; HL, Hybrid Larch; JL, Japanese Larch; SS, Sitka Spruce; MB, Mixed Broadleaves; MC, Mixed Conifers; N/A, Not Applicable.

Table 2
The scoring system applied to classify *P. ramorum* infections.

Score	Foliage Condition	Stem and Branch Condition
NI: Not Infected	No defoliation, discolouration or wilting	No evidence of cankers, resin bleeds or deadwood
1: Light	Defoliation, discolouration or wilting in < 20% of the crown	Cankers may be visible at one or two points on the stem/branches, but a large portion (> 80%) of the stem and branches appear healthy
2: Moderate	Defoliation, discolouration or wilting in 20–80% of the crown	Cankers present and dead branches/portions of the stem may be noted. Between 20% and 80% of the stem/branches affected
3: Heavy	Defoliation, discolouration or wilting in > 80% of the crown	Significant proportions of the main stem/branches visibly affected by infection (cankers, resin bleeds and deadwood) > 80% of the stem and branches affected

in Table 2 was used to separately categorise the foliar and stems symptoms for each tree. The overall severity of *P. ramorum* infection was subsequently determined based on the highest value for the foliage and stem scores. In cases where a reliable survey could not be conducted or there were difficulties sampling suspected plant material, the individual was left uncategorised and removed from the analysis (total of 21 individuals). The selected number and boundaries of disease severity classes used in the scoring system for the study reflects the previously poor performance of remote sensing in the differentiation between classes within the spectrum of moderate disease severity for forest pests (Coops et al., 2003; Leckie et al., 2005). In addition, the management requirements for disease severity data for *P. ramorum* cover two main areas of concern. Firstly, the identification of new infections (category 1) for the issuing of a statutory plant health notice (Tracy, 2009) and secondly, concerns of public safety regarding trees subject to severe decline (category 3) and the associated reductions in structural integrity (Mistretta, 2002; Forestry Commission, 2014).

2.3. ALS data collection

ALS data were acquired for both study sites by Bluesky International via a single aircraft survey utilising the Orion M300 sensor on the 30 June 2015, with an average flight altitude of 1500 m. The scan frequency was 66 Hz, laser pulse repetition frequency was 100 kHz and field-of-view was 8°, beam divergence was 0.25 mrad, sensor range precision was < 8 mm and elevation accuracy was 3–10 cm. Resulting point densities for the Ogmere (infected) and Radnor (control) sites were 20.34 points/m² and 27.39 points/m² respectively, with slight differences in resulting point densities incurred due to small variations in flight altitude.

2.4. Manual delineation

To produce reference polygons for each individual tree, tree crowns were manually delineated. The manual delineation was performed using the ALS-derived data, in addition to photographs and GPS positions for individual trees recorded during ground surveys (Brandtberg and Walter, 1998; Fang et al., 2016). The polygons were applied to the extraction of point cloud and fragmentation metrics from training crowns and used as a basis for determining automated tree crown segmentation accuracy (Pouliot et al., 2002).

Table 3
ALS point cloud metrics extracted from individual trees in the training dataset.

Metric	Definition
Maximum Height	Maximum tree height (m)
Skewness	The skewness of ALS returns above the cut-off height
Bicentiles (B), where N = 10, 20, 30, 40, 50, 60, 70, 80 and 90)	The percentage of ALS returns whose heights are below N% of maximum tree height, after the subtraction of the height cut-off value
Canopy Cover (CC)	The number of first ALS returns above the cut-off height divided by the total number of first ALS returns
Canopy Density (CD)	The number of all ALS returns above the cut-off height divided by the total number of ALS returns

2.5. ALS point cloud metrics

ALS point clouds for individual trees in the training dataset were isolated using the manually delineated polygons. Subsequently, the lascanopy module within LAStools (LAStools, 2016) was used to derive several metrics based on the properties of ALS return pulses (Table 3) from normalised point clouds for each tree (Hopkinson et al., 2016). For example, the bicentiles for individual trees were calculated as the proportion of ALS returns located below a specified percent of tree height (Nevalainen et al., 2017). In order to remove the influence of understorey vegetation, height cut-off values, typically between 1 m and 2 m (Andersen, 2009; Hopkinson et al., 2016; Zellweger et al., 2016), are specified prior to metric calculation. In this study, a static cut-off of 1 m was employed due to the low levels of understorey vegetation across the two study sites. In addition, ALS point cloud metrics were also calculated using a variable cut-off height, set at 50% of tree height, to consider just the characteristics of the upper canopy (Vastaranta et al., 2013). This top portion of the tree canopy is of particular interest for disease detection in the context of the study sites, due to the higher vertical position of the live canopy in coniferous plantation environments with limited thinning management (Macdonald et al., 2009).

2.6. CHM fragmentation metrics

ALS normalised point clouds were used to construct a DTM (ground points) and DSM (maximum of all points) for the two study sites. CHMs were subsequently constructed by the subtraction of the DTM from the DSM (Jakubowski et al., 2013) with a pixel size of 0.15 m. This processing was undertaken in LAStools (LAStools, 2016). For the calculation of fragmentation metrics, CHMs were reclassified based on height. In the two class reclassification, ground and non-ground pixels were distinguished using a threshold value of 0.5 m, this value was selected to minimise the misclassification of ground related pixels. In addition, a three class reclassification was also performed to provide more specific consideration to changes in the lower and upper canopy. In this instance the reclassification applied the 1 m static cut-off value to remove understorey vegetation and considered the maximum tree height value extracted from the CHM using the criteria: ≤ 1 m, > 1 m and ≤ 50% tree height, and > 50% tree height. Following the reclassification of the CHMs, landscape fragmentation metrics were calculated using FRAGSTATS (version 4.2) (McGarigal et al., 2012) for each individual tree within the training dataset. This approach defined the individual tree

Table 4
Landscape fragmentation metrics extracted from individuals in the training dataset.

Metric	Abbrev.	Description
Number of Patches	NP	Number of patches in the landscape
Patch Density	PD	Number of patches in the landscape divided by total landscape area
Largest Patch Index	LPI	The percentage of the landscape covered by the largest patch
Landscape Shape Index	LSI	Standardised measure for the total edge adjusted for the size of landscape
Total Core Area	TCA	Total core area across the landscape
Disjunct Core Area Density	DCAD	The number of disjunct core areas divided by total landscape area
Core Area (Area Weighted Mean)	CORE_AM	Core area for the entire landscape as a percentage of total landscape area
Euclidean Nearest Neighbour (Area Weighted Mean)	ENN_AM	Measure of patch isolation, area weighted mean of the shortest straight line distance between patches
Percentage of Like Adjacencies	PLADJ	Sum of like adjacencies divided by the total number of cell adjacencies in the landscape
Patch Cohesion Index	COHESION	Measure of physical connectedness, using patch perimeter and patch area
Landscape Division Index	DIVISION	The probability that two randomly selected pixels are not situated in the same patch
Patch Richness Density	PRD	Number of different patch types in the landscape divided by the total area of the landscape
Shannon's Diversity Index	SHDI	From the field of ecology, is of indicator or patch diversity in the landscape. More sensitive to rare patch types than Simpson's Index
Simpson's Diversity Index	SIDI	From the field of ecology, is of indicator or patch diversity in the landscape. More intuitive than the Shannon's Index
Aggregation Index	AI	The number of like adjacencies with corresponding class divided by maximum possible number of like adjacencies with corresponding class

crown as the landscape and the height value categories as classes. Table 4 lists all landscape metrics calculated which concern a range of landscape fragmentation measures such as the area-edge relationships, the integrity of core area and the aggregation and diversity of patches within the landscape. Additional information regarding the calculation of metrics can be located in the FRAGSTATS users guide (McGarigal, 2015). An 8-pixel neighbourhood was applied to consider diagonal adjacencies in the definition of patches and in the case of metrics relating to core area a threshold of 1 m was applied.

2.7. Disease severity discrimination

Structural variability in ALS point clouds can also arise as a result of differences in stand age (Ørka et al., 2009). Prior to the disease severity discrimination assessment, a linear regression analysis was conducted to determine any relationships present between the metrics (ALS point cloud and fragmentation) and maximum tree height for individuals from the training dataset at the healthy Radnor Forest. Metrics which reported a significant relationship with tree height were subsequently removed from further analysis and not considered as input variables for the disease severity classification.

To determine the disease severity discrimination potential of the ALS point cloud and fragmentation metrics the Kruskal-Wallis test was applied with Mann-Whitney post hoc tests. The results of the Mann-Whitney post hoc testing were subject to a Bonferroni-Holm correction to limit the overall type I error for multiple testing (Ismail et al., 2007). In this instance, the application of the parametric analysis of variance (ANOVA) followed by Tukey's HSD tests (Coops et al., 2003; Ismail et al., 2007) was not appropriate as several datasets failed to meet the assumptions of normality (Shapiro-Wilk test) or homogeneity of variances (Levene's test). For the purpose of data analysis all individual larch trees without *P. ramorum* have been grouped together to form the not infected (NI) category to be compared with the three disease severity categories (1, 2, and 3).

Table 5
Parameters for filtering and smoothing prior to ITC segmentation.

Maximum Tree Height (m)	Local Maxima Distance Filter (m)	Smoothing Filter (Pixels)	Pixel Size (m)	Min Area Threshold (m ²)
≥ 15	1	5 × 5	0.15	0.5
> 15 and < 30	2	5 × 5	0.25	3
≥ 30	3	5 × 5	0.5	7

2.8. Automated tree crown segmentation

The selected methodology for the automated ITC segmentation of test crowns at the study sites for the disease presence/absence and severity classifications was based on the finding of Barnes et al. (2017). A pit-free CHM was generated using the method specified by Khosravipour et al., 2014, which requires the construction of partial CHMs (2 m, 5 m, 10 m, 15 m and 20 m) which are then stacked in height order and the maximum value for each pixel is used for the generation of the CHM. CHMs were generated at three pixel sizes (0.15 m, 0.25 m and 0.5 m), with the most suitable pixel size for each plot selected on the basis of maximum tree height (Table 5). CHMs were subsequently subject to a low pass smoothing filter followed by the extraction local maxima (> 2 m in height) which were subject to a minimum distance filter, the sizing of both filters was also adjusted in accordance with the maximum tree height of the plot (Table 5). Finally, a marker-controlled watershed segmentation (Wang et al., 2004) was applied using the smoothed pit-free CHM and previously extracted local maxima. Segments which failed to meet the minimum area threshold (Table 5) were merged with the neighbour of the longest common border (Koch et al., 2006). To determine the accuracy of the crown outlines resulting from the ITC segmentation, an automated assessment (Table 6) was conducted to determine the percentage overlap of these automated ITCs with the manually delineated reference crowns for the study areas (Barnes et al., 2017). Segments classified as correct or

Table 6
Assessment categories for the tree crown delineation accuracy analysis.

Category	Description	Percentage overlap (%)			
		R1	R2	A1	A2
Correct	Reference crown dominated by one automated crown	≥ 50	< 2	≥ 50	N/C
Satisfactory	Reference crown largely associated with one automated crown	≥ 50	< 50	≥ 50	< 50
Oversized	Reference crown only accounts for small portion of automated crown	≥ 50	N/C	< 50	N/C
Split	Reference crown dominated by more than one automated crown	N/C	N/C	N/C	≥ 50
Missed	Reference crown has no or poor overlap with automated crowns	< 50	N/C	N/C	< 50

R1: highest overlap percentage for the reference crown; R2: second highest percentage overlap for the reference crown; A1: highest percentage overlap for the automated crown; A2: second highest percentage overlap for the automated crown. Abbreviations: N/C = No conditions.

satisfactory categories (Table 6) were deemed successful for the purpose of the study and overall accuracy percentages were calculated using the ratio of successfully delineated test crowns to the total number of test individuals in sample transects/plots (Hu et al., 2014).

2.9. Classification

Successfully delineated automated ITC polygons for test trees at the study site were subject to classification. Two sets of classification criteria were tested: presence (not infected and infected); and severity (1, 2, 3 and NI) using ALS and fragmentation metrics individually. A combination of ALS and fragmentation metrics as input variables was also considered but this did not yield any improvement in classification. Two distinct classification approaches were used: k-nearest neighbour (k-NN) and random forest (RF). For the implementation of the non-parametric pattern recognition classifier k-NN, the K value, which represents the number of samples considered for the classification of each feature (Collins et al., 2004; Melgani and Bruzzone, 2004; Yu et al., 2006), was established using a grid search cross validation of the training sample testing K values ranging from 1 to 30 (Melgani and Bruzzone, 2004; Hsu et al., 2008).

The second classification method random forest (RF) (Breiman, 2001), is a non-parametric approach which generates a series of classification and regression trees (CART). Each tree is generated using a bootstrapped set of training samples, with the split at each regression tree governed by a randomised subset of input variables for each node (Hudak et al., 2008; Oliveira et al., 2012). The final classification result is subsequently determined based of the highest mean probability estimate across all trees (Belgiu and Drăguț, 2016). Two important input parameters for the RF classification include the number of regression trees (n_{tree}) and the number of input variables at each split in the tree building process (m_{try}). Following a preliminary grid search cross validation of the training dataset, the n_{tree} and m_{try} were set to 500 and 2 respectively, similar to the values applied in previous studies (Immitzer et al., 2012; Ortiz et al., 2013; Shendryk et al., 2016). All processing for the two classification methods was undertaken in Python using Scikit-learn (Pedregosa et al., 2011).

Classification input variables were selected based on the results of the disease severity discrimination analysis and classification performance was reviewed using the overall accuracy percentage (OA) and Cohen's κ coefficient (Cohen, 1960). Interpretation of κ was based on the following categories: ≤ 0.20 is poor; > 0.20 to ≤ 0.40 is fair; > 0.40 to ≤ 0.60 is moderate; > 0.60 to ≤ 0.80 is good; and > 0.80 to ≤ 1 is very good (Landis and Koch, 1977). Confusion matrices were employed to provide a more detailed evaluation of the most successful classifications (Congalton and Green, 1999).

3. Results

3.1. Tree height

In the case of the ALS point cloud metrics significant relationships were evident between the bicultiles B20, B30 and B50 (1 m cut-off height) and tree height (Table 7). All other ALS point cloud metrics did not show significant relationships with tree height. B20, B30 and B50 were therefore removed from further analysis, in addition to B40 which was significant at the 90% confidence level. With regard to the fragmentation metrics (Table 8) significant relationships with tree height were reported for all two class metrics, excluding ENN_AM. For the three class approach, seven metrics (NP, LSI, TCA, CORE_AM, ENN_AM, COHESION and PRD) exhibited a significant relationship with tree height. In light of these results all two class metrics were removed from the disease severity analysis in addition to the seven significant three class metrics, to reduce the potential influence of tree height on the disease severity analysis.

Table 7

Coefficient of determination (R^2) and p values for the linear regression analysis between the ALS metrics and tree height (m) for training data from the healthy Radnor Forest.

ALS Metric	R^2 value		p value	
	1 m COH	50% COH	1 m COH	50% COH
Skewness	0.07	0.05	0.107	0.167
Canopy Cover	< 0.01	< 0.01	0.938	0.847
Canopy Density	0.05	0.02	0.174	0.361
B10	0.01	0.03	0.647	0.314
B20	0.11 [*]	0.03	0.040 [*]	0.320
B30	0.15 [*]	< 0.01	0.015 [*]	0.747
B40	0.09	< 0.01	0.058	0.847
B50	0.11 [*]	0.01	0.043 [*]	0.470
B60	0.06	0.03	0.144	0.280
B70	0.06	0.01	0.120	0.545
B80	0.06	< 0.01	0.144	0.701
B90	< 0.01	0.02	0.597	0.441

Abbreviations: COH – Cut-off height.

* Significant $p < 0.05$.

Table 8

Coefficient of determination (R^2) and p values for the linear regression analysis between the fragmentation metrics and tree height (m) for training data from the healthy Radnor Forest.

Fragmentation Metric	R^2 value		p value	
	2 Class	3 Class	2 Class	3 Class
NP	0.27 [*]	0.45 [*]	0.001 [*]	0.000 [*]
PD	0.27 [*]	0.10	0.001 [*]	0.058
LPI	0.13 [*]	0.10	0.023 [*]	0.058
LSI	0.20 [*]	0.41 [*]	0.005 [*]	0.000 [*]
TCA	0.37 [*]	0.20 [*]	0.000 [*]	0.004 [*]
DCAD	0.18 [*]	0.04	0.007 [*]	0.236
CORE_AM	0.37 [*]	0.16 [*]	0.000 [*]	0.012 [*]
ENN_AM	0.07	0.20 [*]	0.098	0.005 [*]
PLADJ	0.51 [*]	0.09	0.000 [*]	0.064
COHESION	0.22 [*]	0.42 [*]	0.003 [*]	0.000 [*]
DIVISION	0.13 [*]	0.08	0.025 [*]	0.087
PRD	0.54 [*]	0.59 [*]	0.000 [*]	0.000 [*]
SHDI	0.11 [*]	0.02	0.042 [*]	0.380
SIDI	0.14 [*]	0.06	0.021 [*]	0.150
AI	0.17 [*]	0.01	0.009 [*]	0.535

* Significant $p < 0.05$.

3.2. Disease severity discrimination

Fig. 2 shows the ALS profiles and CHMs for four individual trees across the disease severity categories. The ALS profiles demonstrate a larger number of ground or near ground returns for the moderate and heavily infected individuals. In the case of the heavily infected individual, the ALS profile also demonstrates a greater spread of returns across the height of the tree. In addition, the CHMs from diseased trees exhibit a patchier appearance, with an increased presence of low height values towards the centre of the crown for greater levels of infection. The ALS and fragmentation metrics calculated provide a quantification of these observations across all individual trees within the training dataset.

Tables 9 and 10 present the p values from the Kruskal-Wallis test for the disease severity category discrimination for the ALS point cloud metrics and fragmentation metrics respectively. The results from the analysis regarding ALS point cloud metrics demonstrated significant differences in the case of all point cloud metrics at the 50% cut-off height, with the same for the 1 m cut-off height except for in the case of B10. In addition, all fragmentation metrics tested also yielded significant differences between disease severity categories.

To assess the difference in ALS point cloud and fragmentation metrics for the four disease severity categories (NI, 1, 2 and 3) in more

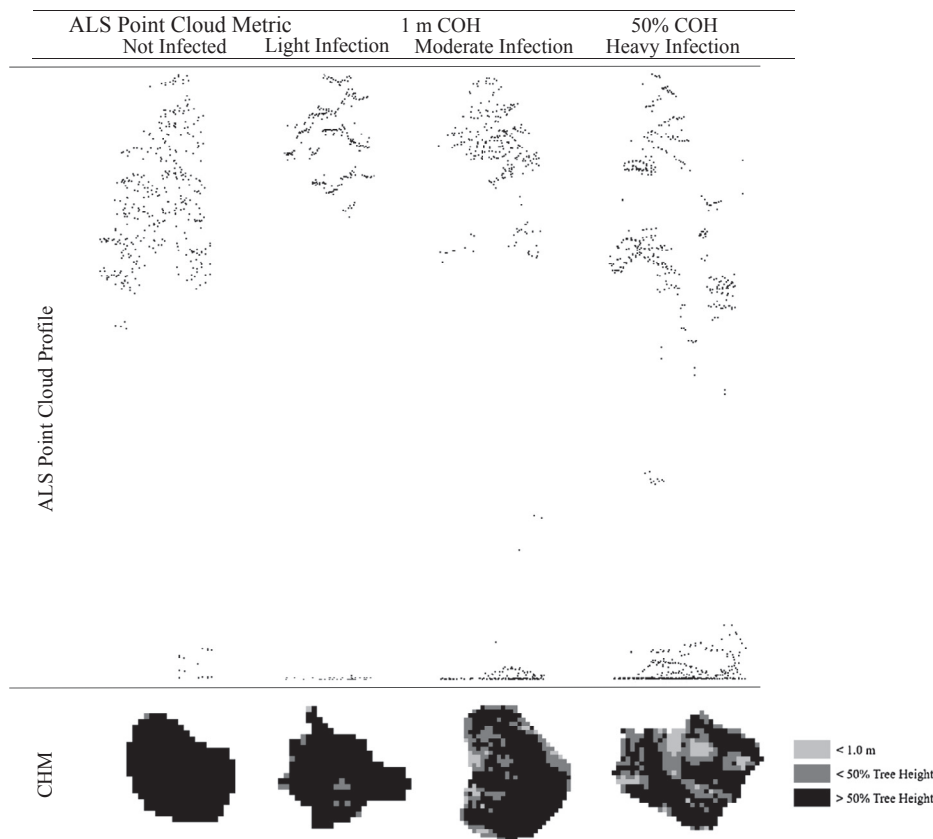


Fig. 2. The top four point clouds demonstrates the ALS vertical profiles for the four disease severity categories. The bottom four images show the horizontal canopy height model classified into three height categories (< 1 m; < 50% tree height; > 50% tree height) for individual trees across the four disease severity categories.

Table 9
Kruskal-Wallis test *p* values for disease severity discrimination from ALS point cloud metrics.

ALS Point Cloud Metric	1 m COH	50% COH
Skewness	0.002*	0.001*
Canopy Cover	< 0.001*	0.002*
Canopy Density	< 0.001*	0.006*
B10	0.487	0.005
B60	0.014*	< 0.001*
B70	0.002*	< 0.001*
B80	0.001*	< 0.001*
B90	< 0.001*	< 0.001*

Abbreviations: COH – Cut-off height.

* Significant *p* < 0.05.

Table 10
Kruskal-Wallis test *p* values for disease severity discrimination from three class fragmentation metrics.

Fragmentation Metric	<i>p</i> value
PD	< 0.001*
LPI	0.001*
DCAD	0.001*
PLADJ	< 0.001*
DIVISION	0.001*
SHDI	< 0.001*
SIDI	0.001*
AI	< 0.001*

* Significant *p* < 0.05

detail, Mann-Whitney post hoc tests with the Bonferroni-Holm correction for multiple comparisons were conducted. Table 11 presents the post hoc test results for the ALS point cloud (1 m and 50% cut-off height) and fragmentation metrics. In the case of the 1 m and 50% cut-

off height ALS metrics, significant differences were collectively observed between all disease severity categories excluding not infected (NI) and light infection (1). All ALS point cloud metrics demonstrated a significant difference between at least one set of disease severity categories except for B10 at the 1 m cut-off height. All of the fragmentation metrics demonstrated significant differences between the disease severity category 3 (heavy infection) and all other severity categories (NI, 1 and 2), except for Disjunct Core Area Density (DCAD) which exhibited significant differences between categories 2 and NI, categories 3 and NI, and categories 2 and 3.

3.3. Automated tree crown segmentation

The results depicted in Table 12 demonstrate the percentage of test crowns successfully delineated via the automated tree crown segmentation. The large variation in successful delineation percentages across the sample areas is caused by the small number of test crowns in some of the plots.

3.4. Disease severity classification

3.4.1. ALS point cloud metrics

Table 13 presents the results from the best k-NN and RF classification of disease presence (infected and not infected) from the ALS point cloud metrics. Overall the best classification was achieved by the k-NN classification of the B80 and B90 (1 m cut-off height). Whilst the resulting κ of 0.32 can be interpreted as a fair classification (Landis and Koch, 1977), the high producer’s accuracy (97.78%) for the not infected (NI) class and low number of false negatives (1) suggest the classification performs well for healthy individuals with most confusion resulting from the classification of infected individuals.

The classification results from the k-NN and RF classifiers for disease severity using the ALS point cloud metrics are displayed in Table 14. Both performed best using the same input variables (50% cut-

Table 11
Mann Whitney (with Bonferroni-Holm correction) post hoc test results for the ALS point cloud metrics at the static 1 m cut-off height and variable 50% cut-off height and fragmentation metrics calculated with the three class reclassification.

		1 m COH				50% COH				Fragmentation 3 Class				
		1	2	3	NI	1	2	3	NI	1	2	3	NI	
1	Skew		****	*	–		****	*	–	PD		–	**	–
2		****		–	*	****		–	*		–		**	
3		*	–		–	*	–		*		**	**		****
NI		–	*	–	–	–	*	*	–		–	–		****
1	CC		–	****	–		–	*	–	LPI		–	***	–
2		–		***	–	–		****	*		–		****	–
3		****	***		****	*	****		**		**	****		****
NI		–	–	****	–	–	*	**	–		–	–		****
1	CD		–	****	–		–	–	–	DCAD		–	–	–
2		–		***	–	–		****	–		–		****	*
3		****	***		****	–	****		**		–	****		**
NI		–	–	****	–	–	–	**	–		–	*	**	–
1	B10		–	–	–		–	*	–	PLADJ		–	****	–
2		–		–	–	–		–	–		–		***	–
3		–	–	–	–	*	–	–	**		****	***		****
NI		–	–	–	–	–	*	**	–		–	–		****
1	B60		*	–	–		***	***	–	DIV.		–	***	–
2		*		–	**	***		–	***		–		****	–
3		–	–	–	–	***	–	–	***		***	****		****
NI		–	**	–	–	–	***	***	–		–	–		****
1	B70		***	–	–		***	****	–	SHDI		–	***	–
2		***		–	**	***		–	***		–		****	–
3		–	–	–	–	****	–	–	***		****	****		****
NI		–	**	–	–	–	***	***	–		–	–		****
1	B80		***	**	–		***	***	–	SIDI		–	**	–
2		***		–	***	***		–	***		–		****	–
3		**	–	–	***	***	–	–	****		****	****		****
NI		–	***	***	–	–	***	****	–		–	–		****
1	B90		**	**	–		–	**	–	AI		–	****	–
2		**		–	****	–		–	***		–		***	–
3		**	–	–	**	**	–	–	****		****	****		****
NI		–	****	**	–	–	**	****	–		–	–		****

Abbreviations: COH – Cut-off height; Skew – Skewness; CC – Canopy Cover; CD – Canopy Density; DIV- DIVISION.

– No significant difference.

* p < 0.10.

** p < 0.05.

*** p < 0.01.

**** p < 0.001.

Table 12
Percentage of successfully delineated test tree crowns for each of the sample plots/transects.

No.	Forest	Maximum Height (m)	Percentage of Test Crowns Successfully Delineated (%)
T1	Ogmore	8.41	63.64
T2	Ogmore	11.54	54.56
P3	Ogmore	18.84	90.91
T4	Ogmore	14.48	42.86
T5	Ogmore	16.64	100.00
T6	Ogmore	20.30	60.00
T7	Ogmore	21.52	60.00
P8	Ogmore	24.59	44.44
T9	Radnor	21.19	80.00
T10	Radnor	6.88	75.00
T11	Radnor	19.58	70.00
T12	Radnor	32.78	100.00
T13	Radnor	33.04	100.00
T14	Radnor	25.49	100.00
T15	Radnor	18.15	25.00
T16	Radnor	26.79	50.00

Table 13
Confusion matrix for best performing k-NN and RF classification of disease presence (infected/not infected) using ALS point cloud metrics.

		k-NN Inputs: 1 m cut-off height B80 and B90			RF Inputs (Feature Importance): 50% cut-off height Skew (0.18), CC (0.17), B60 (0.21), B70 (0.23), B80 (0.21)		
		Classified			Classified		
		NI	IN	PA	NI	IN	PA
Reference	NI	44	1	97.78	26	19	57.78
	IN	19	8	29.63	10	17	62.96
	UA	69.84	88.89		72.22	47.22	
OA (%)		72.22			59.72		
κ		0.32			0.21		

Abbreviations: IN – Infected; NI – Not Infected.

off height: Skewness, Canopy Cover, B60, B70 and B80), with the k-NN classifier producing the highest overall accuracy (65.28%) and κ (0.27), which indicates a fair classification (Landis and Koch, 1977). Assessment of the confusion matrix demonstrated that particular difficulties were encountered with the classification of disease categories 1 and 2 which yielded poor producer’s (14.29%, 28.57%) and user’s (28.57%,

Table 14
Confusion matrix for k-NN and RF classification of disease severity categories (1: Light; 2: Moderate; 3: Heavy; NI: Not Infected) using ALS point cloud metrics.

	k-NN Input: 50% cut-off height Skewness, Canopy Cover, B60, B70, B80 Classified					RF Input (Feature Importance): 50% cut-off height Skewness (0.18), Canopy Cover (0.23), B60 (0.18), B70 (0.23), B80 (0.19). Classified					
	1	2	3	NI	PA	1	2	3	NI	PA	
Reference	1	2	0	0	12	14.29	5	0	2	7	35.71
	2	1	2	0	4	28.57	2	1	1	3	14.29
	3	0	2	3	1	50	0	0	5	1	83.33
	NI	4	1	0	40	88.89	6	2	10	27	60
	UA	28.57	40	100	70.18	38.46	33.33	27.78	71.05		
OA (%)						65.28					
κ						0.27					

Table 15
Confusion matrix for k-NN and RF classification of disease presence using all three class fragmentation metrics.

	k-NN Classified			RF Classified			
	NI	IN	PA	NI	IN	PA	
Reference	NI	40	5	88.89	19	26	42.22
	IN	20	7	25.93	5	22	81.48
	UA	66.67	58.33	79.17	45.83		
OA (%)	65.28			56.94			
κ	0.17			0.21			

RF feature importance: PD (0.15), LPI (0.09), DCAD (0.13), PLADJ (0.16), DIV (0.11), SHDI (0.12), SIDI (0.10), AI (0.13). Abbreviations: IN – Infected; NI – Not Infected.

40.00%) accuracies.

3.4.2. Fragmentation metrics

All the classification results in Tables 15 and 16 were achieved using all eight three class fragmentation metrics as input variables. In the case of the disease presence classification (Table 15), the k-NN classifier resulted in greatest overall accuracy (65.28%), whilst the RF classifier produced the highest κ at 0.21. The RF confusion matrix exhibited a low number of false negatives, with the majority of confusion resulting from false positives. In the case of the disease severity classification (Table 16), the k-NN classifier was responsible for the best classification (OA = 68.06% and κ = 0.24). Difficulties in identifying categories 1 and 2 were clearly apparent with producer’s and user’s accuracies for both classes report as 0%. Consideration was given to combing the ALS and fragmentation metrics but this did not improve the classification accuracies of disease presence or severity.

Table 16
Confusion matrix for k-NN and RF classification of disease severity using all three class fragmentation metrics.

	k-NN Classified					RF Classified					
	1	2	3	NI	PA	1	2	3	NI	PA	
Reference	1	0	0	0	14	0	8	1	2	3	57.14
	2	0	0	0	7	0	2	0	2	3	0
	3	0	0	5	1	83.33	1	0	5	0	83.33
	NI	1	0	0	44	97.78	20	0	2	23	51.11
	UA	0	0	100	66.67	25.81	0	45.45	79.31		
OA (%)	68.06					50					
κ	0.24					0.23					

RF feature importance: PD (0.14), LPI (0.09), DCAD (0.11), PLADJ (0.16), DIV (0.12), SHDI (0.12), SIDI (0.11), AI (0.15).

3.4.3. Classification limitations

In the case of the disease presence/absence and severity classifications performed using both the ALS point cloud and fragmentation metrics, several key limitations require acknowledgement. Firstly, the small number of samples from each of the categories, especially in the case of the categories 2 (moderate) and 3 (heavy), fell below the recommended minimum threshold for a statistically valid assessment (Van Genderen and Lock, 1977; Congalton, 1991), influencing the predictive capabilities of the classifiers (Melgani and Bruzzone, 2004; Belgiu and Drăguț, 2016). In addition, the number of samples in each of the disease presence and severity categories was also unbalanced, providing potential difficulties in the ability of the classifiers to accurately separate individual classes (Muñoz-Marí et al., 2007; Belgiu and Drăguț, 2016).

4. Discussion

The results highlighted the presence of a linear relationship between some of the ALS point cloud and fragmentation metrics and tree height, demonstrating the influence of tree growth and canopy development on the structure and character of healthy larch crowns. For example, contrasts between crown height and density of foliage in younger and older stands can provide a different signal in metrics calculated from ALS for healthy individuals. The influence of tree height relationships for disease detection purposes in larch can be avoided for the ALS point cloud metrics when a variable cut-off height (50%) based on tree height is applied. However, significant relationships between fragmentation metrics and tree height were evident for both the two and three class approaches, although less fragmentation metrics exhibited a significant relationship in the case of the three class methodology which was selected for disease discrimination analysis. Resultantly, tree height demonstrates a dominant influence controlling the ALS and fragmentation metrics produced for individual trees and requires consideration in analysis regarding disease detection and assessment.

The disease severity discrimination analysis revealed that collectively, ALS point cloud metrics exhibited significantly different values for all disease severity categories except in the case of the not infected (NI) and light infection (1) categories. This highlights that structural canopy changes as the result of *P. ramorum* infection in the later stage of disease progression (categories 2 and 3) can be detected via the application of ALS point cloud metrics at the individual tree crown scale. This supports the findings of previous research regarding insect pests of coniferous tree species, which noted an increased penetration of ALS pulses through the canopy and a greater portion of ground returns for canopies subject to defoliation as a result of insect attack (Coops et al., 2009; Bright et al., 2013). The difficulties noted with regard to the separation of not infected individuals and those in the early stages of infection has also been previously recognised within the literature (Bater et al., 2010; Kantola et al., 2010). The results from this study

indicate that even with high ALS point densities, metrics derived from ALS point clouds are unable to detect the very slight changes in canopy structure which are encountered in the early onset of the *P. ramorum* infection. In addition, discrete return ALS biases the resulting datasets against foliage located in the middle of the tree crown (Lovell et al., 2003). As a result, when early stages of infection are not present in the top of the canopy, detection via the application of discrete ALS point cloud metrics may also be more difficult.

The results from the disease severity discrimination analysis for the fragmentation metrics demonstrate the potential applications of this group of metrics for the assessment of severe decline in ITC condition. Whilst significant differences were only consistently noted to provide separation of heavily infected individuals (category 3) with all other severity categories, this is likely to result from the CHMs representation of the canopy surface and the requirement of upper canopy fragmentation for disease detection. Nevertheless, the results indicate the previously untested value of CHM raster data for disease assessment in the absence of the original point cloud. Such results are also of particular interest from the perspective of dead wood mapping in forest environments (Martinuzzi et al., 2009; Pasher and King, 2009). The presence of significant results from a range of fragmentation metrics suggests in heavily infected larch trees (category 3) changes in ALS penetration across the upper canopy (Coops et al., 2009; Bright et al., 2013) can alter resulting height values in CHMs to a large enough extent to increase the fragmentation of height value classes in tree crowns. This effect changes the characteristics of core areas as well as increasing the complexity of height value patches in the tree crown landscape. The contrast in the mosaic of height class patches between heavily infected and healthy tree crowns is sufficient to provide a means of separating these individuals (Du-ning and Xiu-zhen, 1999). Nevertheless, the high point density of the ALS (24 points/m²) facilitated the generation of the high resolution CHM (0.15 m) applied in this study. Further investigation is subsequently required to determine whether the same level of discrimination can be achieved for CHMs of a lower resolution (> 0.15 m).

The results of the disease presence (not infected/infected) classification provided a straightforward indication of the value of ALS datasets for the detection of *P. ramorum* in larch species. The results indicated that the application of a k-NN classifier to ALS point cloud metrics (B80 and B90 1 m cut-off height) could provide fair classification ($\kappa = 0.32$), with an acceptable overall accuracy (72.22%). The greatest limitation of this classification is the poor performance of the infected classification (producer's accuracy 29.63%). Given the results of the disease severity discrimination with the Mann-Whitney post hoc analysis, it is likely that discriminating individuals within the not infected (NI) and light infection (category 1) categories are causing the greatest confusion. Kantola et al. (2010) set a defoliation level of 20% or more for their classification of Scots pine (*Pinus sylvestris*) defoliated by the common pine sawfly (*Diprion pini*). Acknowledging the limitations of the approach for the detection of individuals in the early stages of *P. ramorum* infection, a higher threshold of defoliation could be employed for operational use during disease detection. A defoliation threshold was not applied in this study as it was important to assess the overall success of ALS across the spectrum of *P. ramorum* disease severities. With regard to the superior performance of the k-NN in comparison to the RF classifier, the less complex application of two input variables (B80 and B90 1 m cut-off height) with a cross validated K value (Latifi et al., 2010) provided a better binary classification of *P. ramorum* infection than the more complex RF (McInerney and Nieuwenhuis, 2009). The impacts of low sample size and an unbalanced number of samples across the two categories may also have limited the classification performance of the RF classifier (Belgiu and Drăguț, 2016).

The results from the disease severity classification yielded a fair classification ($\kappa = 0.23$ – 0.27), however no classifier or input metrics (ALS point cloud or fragmentation) demonstrated a superior

performance over the other. Assessment of the confusion matrices revealed that classification of the infected disease severity classes 1 and 2 were often the most problematic. Whilst classes in this study represented key areas of interest during the disease progression, each class exhibits a spectrum of crown conditions, causing difficulty in separating disease severity at specified threshold levels (Coops et al., 2003). The use of automated polygons representing tree crowns also results in further complications with regard to the extraction ALS and fragmentation metrics from the test crowns for classification. For example, whilst some overlap perfectly with ITCs, those categorised as satisfactory may incorporate returns from neighbouring vegetation, potentially influencing the calculation of metrics employed as input variables. This effect could be managed with more restrictive criteria, such as 60% or 70% minimum overlap, for determining successfully delineated automated crowns (Shendryk et al., 2016).

The overall classification accuracy of ALS metrics for discrimination of healthy and infected individuals was slightly below the 80.7% achieved for Scots pine (*Pinus sylvestris*) infected by the insect pest the common pine sawfly (*Diprion pini* L) (Kantola et al., 2010). Nevertheless, the research presents the detection capabilities of ALS across the full spectrum of *P. ramorum* infection, including consideration for individuals in the early stage of infection. In addition, the characteristic impacts of each pest and phytopathogen on canopy structure is not uniform and direct comparison does not consider variations in pest/pathogen host interactions, symptom expression and species crown architecture (Lovett et al., 2006).

These results highlight the application of previously untested fragmentation metrics for the quantification the increased patchiness of tree crown CHMs subject to heavy *P. ramorum* infection. Whilst the results indicate the preferable application of ALS point cloud datasets for the assessment of *P. ramorum*, the availability of original datasets, expertise and resources for processing may present barriers in the operational applications of ALS in forestry. Therefore, a range of approaches to the application of ALS to disease assessment provides flexibility for forest management (Suárez et al., 2005; Hall et al., 2016).

Further consideration for the application of ALS to the detection and assessment of *P. ramorum* infection in larch should take into account the point density of ALS datasets. Whilst the point density applied in this instance (24 points/m²) can be considered high, low density datasets cannot be presumed to provide the same results (Kantola et al., 2010). Furthermore, as suggested by Coops et al. (2009), further understanding of the impact of disease on ALS point cloud metrics could be established with the application of pre and post infection ALS datasets. Such assessment can also be applied in the case of CHMs (Vastaranta et al., 2012). To fully assess the potential benefits of an approach based on remote sensing data in comparison to those presently achieved manually by visual assessment, a comparison between the two approaches would also be valuable to provide additional merit to a remote sensing approach.

5. Conclusion

The research demonstrates the successful application of ALS point cloud metrics to isolate individual tree crowns of larch subject to moderate (category 2) and severe (category 3) *P. ramorum* infection based on the impacts of the disease on individual tree crown canopy structure. The results also highlight the merits of CHMs alone for isolating heavily infected individuals (category 3) via the first assessment of fragmentation metrics to quantify the patchiness exhibited by diseased tree crowns. Overall classification of disease presence and severity were best achieved using a k-NN classifier with percentages of 72.22% and 65.28% respectively. κ values for disease presence and severity of 0.32 and 0.27 respectively indicated a fair classification, with low values as a result of poor classification for infected individuals particularly those within the early stages of infection (category 1). Whilst higher accuracies could be achieved by raising the threshold of

symptomatic material for infected individuals, it was important to highlight the performance of ALS across the whole spectrum of *P. ramorum* infection levels. For operational applications regarding disease assessment in larch forests, the limitations of the technique in identifying individual tree crowns subject to the early stages of disease establishment requires acknowledgment.

Funding Sources

The work was funded as part of a NERC CASE studentship (NE/L008068/1) with partner Bluesky International who collected the ALS data for the research.

Appendix A. Supplementary material

Supplementary data associated with this article can be found, in the online version, at <http://dx.doi.org/10.1016/j.foreco.2017.08.052>.

References

- Andersen, H.E., 2009. Using airborne light detection and ranging (LIDAR) to characterize forest stand condition on the Kenai Peninsula of Alaska. *Western J. Appl. Forest.* 24 (2), 95–102.
- Balzter, H., Luckman, A., Skinner, L., Rowland, C., Dawson, T., 2007. Observations of forest stand top height and mean height from interferometric SAR and LiDAR over a conifer plantation at Thetford Forest, UK. *Int. J. Remote Sens.* 28 (6), 1173–1197.
- Barnes, C., Balzter, H., Barrett, K., Eddy, J., Milner, S., Suárez, J.C., 2017. Individual tree crown delineation from airborne laser scanning for diseased larch forest stands. *Remote Sens.* 9 (3), 231.
- Bater, C.W., Wulder, M.A., White, J.C., Coops, N.C., 2010. Integration of LiDAR and digital aerial imagery for detailed estimates of lodgepole pine (*Pinus contorta*) volume killed by mountain pine beetle (*Dendroctonus ponderosae*). *J. Forest.* 108 (3), 111–119.
- Belgiu, M., Drăguț, L., 2016. Random forest in remote sensing: a review of applications and future directions. *ISPRS J. Photogramm. Remote Sens.* 114, 24–31.
- Ben-Arie, J.R., Hay, G.J., Powers, R.P., Castilla, G., St-Onge, B., 2009. Development of a pit filling algorithm for LiDAR canopy height models. *Comput. Geosci.* 35, 1940–1949.
- Brandtberg, T., Walter, F., 1998. Automated delineation of individual tree crowns in high spatial resolution aerial images by multiple-scale analysis. *Mach. Vis. Appl.* 11 (2), 64–73.
- Brandtberg, T., Warner, T.A., Landenberger, R.E., McGraw, J.B., 2003. Detection and analysis of individual leaf-off tree crowns in small footprint, high sampling density lidar data from the eastern deciduous forest in North America. *Remote Sens. Environ.* 85, 290–303.
- Brasier, C.M., 2008. The biosecurity threat to the UK and global environment from international trade in plants. *Plant. Pathol.* 57 (5), 792–808.
- Breidenbach, J., Naeset, E., Lien, V., Gobakken, T., Solberg, S., 2010. Prediction of species specific forest inventory attributes using a nonparametric semi-individual tree crown approach based on fused airborne laser scanning and multispectral data. *Remote Sens. Environ.* 114 (4), 911–924.
- Breiman, L., 2001. Random forests. *Mach. Learn.* 45, 5–32.
- Bright, B.C., Hudak, A.T., McGaughey, R., Andersen, H.E., Negrón, J., 2013. Predicting live and dead tree basal area of bark beetle affected forests from discrete-return lidar. *Can. J. Remote. Sens.* 39, S1–S13.
- Brown, A.V., Rose, D.R., Webber, J.F., 2003. Red Band Needle Blight of Pine. Forestry Commission: Forest Research Information Note 49, Edinburgh, UK.
- Casas, A., García, M., Siegel, R.B., Koltunov, A., Ramirez, C., Ustin, S., 2016. Burned forest characterization at single-tree level with airborne laser scanning for assessing wildlife habitat. *Remote Sens. Environ.* 175, 231–241.
- Cohen, J., 1960. A coefficient of agreement for nominal scales. *Educ. Psychol. Measur.* 20 (1), 37–46.
- Collins, M.J., Dymond, C., Johnson, E.A., 2004. Mapping subalpine forest types using networks of nearest neighbour classifiers. *Int. J. Remote Sens.* 25 (9), 1701–1721.
- Congalton, R.G., 1991. A review of assessing the accuracy of classifications of remotely sensed data. *Remote Sens. Environ.* 37, 35–46.
- Congalton, R., Green, K., 1999. Assessing the Accuracy of Remotely Sensed Data: Principles and Practises. CRC/Lewis Press, Boca Raton, FL, pp. 137.
- Coops, N., Stanford, M., Old, K., Dudzinski, M., Culvenor, D., Stone, C., 2003. Assessment of Dorthistroma needle blight of *Pinus radiata* using airborne hyperspectral imagery. *Phytopathology* 93 (12), 1524–1532.
- Coops, N.C., Varhola, A., Bater, C.W., Teti, P., Boon, S., Goodwin, N., Weiler, M., 2009. Assessing differences in tree and stand structure following beetle infestation using lidar data. *Can. J. Remote. Sens.* 35 (6), 497–508.
- Du-ning, X., Xiu-zhen, L., 1999. Core concepts of landscape ecology. *J. Environ. Sci.* 11 (2), 131–135.
- Dubayah, R.O., Drake, J.B., 2000. Lidar remote sensing for forestry. *J. Forest.* 98 (6), 44–46.
- Fang, F., Im, J., Lee, J., Kim, K., 2016. An improved tree crown delineation method based on live crown ratios from airborne LiDAR data. *GIScience Remote Sens.* 53 (3), 402–419.
- Forestry Commission, 2016. *Phytophthora ramorum outbreak and risk zones maps*. < <http://www.forestry.gov.uk/forestry/infnd-86ajjq> > (accessed on 11/03/16).
- Forestry Commission, 2014. *Tree pests and diseases*. Available at: < <http://www.forestry.gov.uk/forestry/INFDF-6ABL5V> > (accessed on 17/03/15).
- Hall, R.J., Castilla, G., White, J.C., Cooke, B.J., Skakun, R.S., 2016. Remote sensing of forest pest damage: a review and lessons learned from a Canadian perspective. *Can. Entomol.* 148, S296–S356.
- Hargis, C.D., Bissonette, J.A., David, J.L., 1998. The behaviour of landscape metrics commonly used in the study of habitat fragmentation. *Landscape Ecol.* 13, 167–186.
- Holdenrieder, O., Pautasso, M., Weisberg, P.J., Lonsdale, D., 2004. Tree diseases and landscape processes: the challenge of landscape pathology. *Trends Ecol. Evol.* 19 (8), 446–452.
- Holmgren, J., Persson, A., 2004. Identifying species of individual trees using airborne laser scanner. *Remote Sens. Environ.* 90 (4), 415–423.
- Hopkinson, C., Chasmer, L., Gynan, C., Mahoney, C., Sitar, M., 2016. Multisensor and multispectral lidar characterization and classification of a forest environment. *Can. J. Remote. Sens.* 42, 501–520.
- Hsu, C.W., Chang, C.C., Lin, C.J., 2008. A practical guide to support vector classification. Technical Report. Department of Computer Science, National Taiwan University, Taipei 106, Taiwan.
- Hu, B., Li, J., Jing, L., Judah, A., 2014. Improving the efficiency and accuracy of individual tree crown delineation from high-density LiDAR data. *Int. J. Appl. Earth Obs. Geoinf.* 26, 145–155.
- Huang, C., Davis, L.S., Townshend, J.R.G., 2002. An assessment of support vector machines for land cover classification. *Int. J. Remote Sens.* 23 (4), 725–749.
- Hudak, A.T., Crookston, N.L., Evans, J.S., Hall, D.E., Falkowski, M.J., 2008. Nearest neighbour imputation of species-level, plot-scale forest structure attributes from LiDAR data. *Remote Sens. Environ.* 112 (5), 2232–2245.
- Immitzer, M., Atzberger, C., Koukal, T., 2012. Tree species classification with random forest using very high spatial resolution 8-band WorldView-2 satellite data. *Remote Sens.* 4 (9), 2661–2693.
- Ismail, R., Mutanga, O., Bob, U., 2007. Forest health and vitality: the detection and monitoring of *Pinus patula* trees infected by *Sirex noctilio* using digital multispectral imagery. *Southern Hemisphere Forest. J.* 69 (1), 39–47.
- Jakubowski, M.K., Li, W., Guo, Q., Kelly, M., 2013. Delineating individual trees from LiDAR data: a comparison of vector- and raster-based segmentation approaches. *Remote Sens.* 5 (9), 4163–4186.
- Kantola, T., Vastaranta, M., Yu, X., Lyytikäinen-Saarenmaa, P., Holopainen, M., Talvitie, M., Kaasalainen, S., Solberg, S., Hyypä, J., 2010. Classification of defoliated trees using tree-level airborne laser scanning data combined with aerial images. *Remote Sens.* 2 (12), 2665–2679.
- Khosravipour, A., Skidmore, A.K., Isenburg, M., Wang, T., Hussin, Y.A., 2014. Generating pit-free canopy height models from airborne lidar. *Photogramm. Eng. Remote Sens.* 80 (9), 863–872.
- Kim, Y., Yang, Z., Cohen, W.B., Pflugmacher, D., Lauver, C.L., Vankat, J.L., 2009. Distinguishing between live and dead standing tree biomass on the North Rim of Grand Canyon National Park, USA using small-footprint lidar data. *Remote Sens. Environ.* 113 (11), 2499–2510.
- Koch, B., Heyder, U., Weinacker, H., 2006. Detection of individual tree crowns in airborne lidar data. *Photogramm. Eng. Remote Sens.* 72 (4), 357–363.
- Kox, L.F.F., Brouwershaven, I.V., Vossenbergh, B.V.D., Beld, H.V.D., Bonants, P.J.M., Gruyter, J.D., 2007. Diagnostic values and utility of immunological, morphological, and molecular methods for in planta detection of *Phytophthora ramorum*. *Phytopathology* 97 (9), 1119–1129.
- Kupfer, J.A., 2012. Landscape ecology and biogeography: rethinking landscape metrics in a post-FRAGSTATS landscape. *Prog. Phys. Geogr.* 36 (3), 400–420.
- Kwak, D.A., Chung, J., Lee, W.K., Kafatis, M., Lee, S.Y., Cho, H.K., Lee, S.H., 2010. Evaluation for damaged degree of vegetation by forest fire using Lidar and a digital aerial photograph. *Photogramm. Eng. Remote Sens.* 76 (3), 277–287.
- Lane, C.R., Beales, P.A., Hughes, K.J.D., Griffin, R.L., Munro, D., Brasier, C.M., Webber, J.F., 2003. First outbreak of *Phytophthora ramorum* in England, on *Viburnum tinus*. *Plant. Pathol.* 52, 414.
- Landis, J.R., Koch, G.G., 1977. The measurement of observer agreement for categorical data. *Biometrics* 33, 159–174.
- LAStools, 2016. LAStools. < <https://rapidlasso.com/lastools/> > (Accessed on 01/06/16).
- Latifi, H., Nothdurft, A., Koch, B., 2010. Non-parametric prediction and mapping of standing timber volume and biomass in a temperate forest: application of multiple optical/LiDAR-derived predictors. *Forestry* 83 (4), 395–407.
- Lausch, A., Erasmí, S., King, D.J., Magdon, P., Heurich, M., 2017. Understanding forest health with remote sensing-part II – a review of approaches and data models. *Remote Sens.* 9 (2), 129.
- Leckie, D.G., Cloney, E., Joyce, S.P., 2005. Automated detection and mapping of crown discoloration caused by jack pine budworm with 2.5 m resolution multispectral imagery. *Int. J. Appl. Earth Obs. Geoinf.* 7, 61–77.
- Lim, K., Treitz, P., Wulder, M., St-Onge, B., Flood, M., 2003. LiDAR remote sensing of forest structure. *Prog. Phys. Geogr.* 27 (1), 88–106.
- Lovell, J.L., Jupp, D.L., Culvenor, D.S., Coops, N.C., 2003. Using airborne and ground-based ranging lidar to measure canopy structure in Australian forests. *Can. J. Remote. Sens.* 29 (5), 607–622.
- Lovett, G.M., Canham, C.D., Arthur, M.A., Weathers, K.C., Fitzhugh, R.D., 2006. Forest ecosystem responses to exotic pests and pathogens in eastern North America. *Bioscience* 56 (5), 395–405.
- Macdonald, E., Gardiner, B., Mason, W., 2009. The effects of transformation of even-aged stands to continuous cover forestry on conifer log quality and wood properties in the UK. *Forestry* 83 (1), 1–16.

- Martinuzzi, S., Vierling, L.A., Gould, W.A., Falkowski, M.J., Evans, J.S., Hudak, A.T., Vierling, K.T., 2009. Mapping snags and understory shrubs for a LiDAR-based assessment of wildlife habitat suitability. *Remote Sens. Environ.* 113 (12), 2533–2546.
- McGarigal, K., 2015. FRAGSTATS Help [pdf]. Available at: < <https://www.umass.edu/landeco/research/fragstats/documents/fragstats.help.4.2.pdf> > (accessed on 01.12.16).
- McGarigal, K., Cushman, S.A., Ene, E., 2012. FRAGSTATS v4: Spatial Pattern Analysis Program for Categorical and Continuous Maps. Available at: < . Computer software program produced by the authors at the University of Massachusetts, Amherst > (accessed on 01.12.16).
- McInerney, D.O., Nieuwenhuis, M., 2009. A comparative analysis of k NN and decision tree methods for the Irish National Forest Inventory. *Int. J. Remote Sens.* 30 (19), 4937–4955.
- Medcalf, K.A., Bodevin, N., Cameron, I., Webber, J., Turton, N., 2011. Assessing the potential of using remote sensing in support of current *Phytophthora* work. Report to FERA. < http://www.envsys.co.uk/wp-content/uploads/2015/02/Remote_Sensing_Phytophthora.pdf > (accessed 08/03/16).
- Melgani, F., Bruzzone, L., 2004. Classification of hyperspectral remote sensing images with support vector machines. *IEEE Trans. Geosci. Remote Sens.* 42 (8), 1778–1790.
- Mistretta, P.A., 2002. Southern forest resource assessment highlights: managing for forest health. *J. Forest.* 100 (7), 24–27.
- Mitchell, R.J., Beaton, J.K., Bellamy, P.E., Broome, A., Chetcuti, J., Eaton, S., Ellis, C.J., Gimona, A., Harmer, R., Hester, A.J., Hewison, R.L., Hodgetts, N.G., Iason, G.R., Kerr, G., Littlewood, N.A., Newey, S., Potts, J.M., Pozsgai, G., Ray, D., Sim, D.A., Stockan, J.A., Taylor, A.F.S., Woodward, S., 2014. Ash dieback in the UK: a review of the ecological and conservation implications and potential management options. *Biol. Cons.* 175, 95–109.
- Muñoz-Marí, J., Bruzzone, L., Camps-Valls, G., 2007. A support vector domain description approach to supervised classification of remote sensing images. *IEEE Trans. Geosci. Remote Sens.* 45 (8), 2683–2692.
- Nevalainen, O., Honkavaara, E., Tuominen, S., Viljanen, N., Hakala, T., Yu, X., Hyypä, J., Saari, H., Pölonen, I., Imai, N.N., Tommaselli, A.M.G., 2017. Individual tree detection and classification with UAV-based photogrammetric point clouds and hyperspectral imaging. *Remote Sens.* 9 (3), 185.
- Nutter, F., van Rij, N., Eggenberger, S.K., Holah, N., 2010. Spatial and temporal dynamics of plant pathogens. In: Oerke, E.C., Gerhards, R., Menz, G., Sikora, R.A. (Eds.), *Precision crop protection the challenge and use of heterogeneity*. Springer, Dordrecht Chapter 3.
- Oliveira, S., Oehler, F., San-Miguel-Ayanz, J., Camia, A., Pereira, J.M., 2012. Modeling spatial patterns of fire occurrence in Mediterranean Europe using multiple regression and random forest. *Forest Ecol. Manage.* 275, 117–129.
- Ørka, H.O., Næsset, E., Bollandsås, O.M., 2009. Classifying species of individual trees by intensity and structure features derived from airborne laser scanner data. *Remote Sens. Environ.* 113 (6), 1163–1174.
- Ortiz, S.M., Breidenbach, J., Kändler, G., 2013. Early detection of bark beetle green attack using TerraSAR-X and RapidEye data. *Remote Sens.* 5 (4), 1912–1931.
- Pasher, J., King, D.J., 2009. Mapping dead wood distribution in a temperate hardwood forest using high resolution airborne imagery. *For. Ecol. Manage.* 258, 1536–1548.
- Pedregosa, F., Varoquaux, G., Gramfort, A., Michel, V., Thirion, B., Grisel, O., Blondel, M., Prettenhofer, P., Weiss, R., Dubourg, V., Vanderplas, J., 2011. Scikit-learn: machine learning in python. *J. Mach. Learn. Res.* 12, 2825–2830.
- Popescu, S.C., Wynne, R.H., Nelson, R.F., 2003. Measuring individual tree crown diameter with lidar and assessing its influence on estimating forest volume and biomass. *Can. J. Remote. Sens.* 29 (5), 564–577.
- Pouliot, D.A., King, D.J., Bell, F.W., Pitt, D.G., 2002. Automated tree crown detection and delineation in high-resolution digital camera imagery of coniferous forest regeneration. *Remote Sens. Environ.* 82 (2), 322–324.
- Reutebuch, S.E., Andersen, H.E., McGaughey, R.J., 2005. Light detection and ranging (LIDAR): an emerging tool for multiple resource inventory. *J. Forest.* 103 (6), 286–292.
- Rullan-Silva, C.D., Olthoff, A.E., de la Mata, J.D., Pajares-Alonso, J.A., 2013. Remote monitoring of forest insect defoliation—a review. *Forest Syst.* 22 (3), 377–391.
- Samaniego, L., Bárdossy, A., Schulz, K., 2008. Supervised classification of remotely sensed imagery using a modified k-NN technique. *IEEE Trans. Geosci. Remote Sens.* 46 (7), 2112–2125.
- Shendryk, I., Broich, M., Tulbure, M.G., McGrath, A., Keith, D., Alexandrov, S.V., 2016. Mapping individual tree health using full-waveform airborne laser scans and imaging spectroscopy: a case study for floodplain eucalypt forest. *Remote Sens. Environ.* 187, 202–217.
- Sheridan, R.D., Popescu, S.C., Gatzolis, D., Morgan, C.L.S., Ku, N.W., 2015. Modeling forest aboveground biomass and volume using airborne LiDAR metrics and forest inventory and analysis data in the Pacific Northwest. *Remote Sens.* 7 (1), 229–255.
- Solberg, S., Naesset, E., Hanssen, K.H., Christiansen, E., 2006. Mapping defoliation during a severe insect attack on Scots pine using airborne laser scanning. *Remote Sens. Environ.* 102 (3), 364–376.
- Suárez, J.C., Ontiveros, C., Smith, S., Snape, S., 2005. Use of airborne LiDAR and aerial photography in the estimation of individual tree heights in forestry. *Comput. Geosci.* 31 (2), 253–262.
- Tracy, D.R., 2009. *Phytophthora ramorum* and *Phytophthora kernoviae*: the woodland perspective. *EPP Bull.* 39 (2), 161–167.
- Van Genderen, J.L., Lock, B.F., 1977. Testing land-use map accuracy. *Photogramm. Eng. Remote Sens.* 43 (9), 1135–1137.
- Vastaranta, M., Kantola, T., Lyytikäinen-Saarenmaa, P., Holopainen, M., Kankare, V., Wulder, M.A., Hyypä, J., Hyypä, H., 2013. Area-based mapping of defoliation of Scots pine stands using airborne scanning LiDAR. *Remote Sens.* 5 (3), 1220–1234.
- Vastaranta, M., Korpela, I., Uotila, A., Hovi, A., Holopainen, M., 2012. Mapping of snow-damaged trees based on bitemporal airborne LiDAR data. *Eur. J. Forest Res.* 131 (4), 1217–1228.
- Wang, L., Gong, P., Biging, G.S., 2004. Individual tree-crown delineation and treetop detection in high-spatial-resolution aerial imagery. *Photogramm. Eng. Remote Sens.* 70 (3), 351–357.
- Webber, J.F., Mullett, M., Brasier, C.M., 2010. Dieback and mortality of plantation Japanese larch (*Larix kaempferi*) associated with infection by *Phytophthora ramorum*. *New Disease Rep.* 22, 19.
- Webber, J.F., Parkinson, N.M., Rose, J., Stanford, H., Cook, R.T.A., Elphinstone, J.G., 2008. Isolation and identification of *Pseudomonas syringae* pv. *aesculi* causing bleeding canker of horse chestnut in the UK. *Plant. Pathol.* 57 (2) 368–368.
- Wing, B.M., Ritchie, M.W., Boston, K., Cohen, W.B., Oslen, M.J., 2015. Individual snag detection using neighbourhood attribute filtered airborne lidar data. *Remote Sens. Environ.* 163, 165–179.
- Wulder, M.A., Coops, N.C., Hudak, A.T., Morsdorf, F., Nelson, R., Newnham, G., Vastaranta, M., 2013. Status and prospects for LiDAR remote sensing of forested ecosystems. *Can. J. Remote. Sens.* 39, S1–S5.
- Wulder, M.A., Dymond, C.C., White, J.C., Leckie, D.G., Carroll, A.L., 2006. Surveying mountain pine beetle damage of forests: a review of remote sensing opportunities. *For. Ecol. Manage.* 221, 27–41.
- Yoga, S., Bégin, J., St-Onge, B., Gatzolis, D., 2017. Lidar and multispectral imagery classifications of balsam fir tree status for accurate predictions of merchantable volume. *Forests* 8, 253.
- Yu, Q., Gong, P., Clinton, N., Biging, G., Kelly, M., Schirokauer, D., 2006. Object-based detailed vegetation classification with airborne high spatial resolution remote sensing imagery. *Photogramm. Eng. Remote Sens.* 72 (7), 799–811.
- Zellweger, F., Baltensweiler, A., Ginzler, C., Roth, T., Braunisch, V., Bugmann, H., Bollmann, K., 2016. Environmental predictors of species richness in forest landscapes: abiotic factors versus vegetation structure. *J. Biogeogr.* 43 (6), 1080–1090.
- Zimble, D.A., Evans, D.L., Carlson, G.C., Parker, R.C., Grado, S.C., Gerard, P.D., 2003. Characterizing vertical forest structure using small-footprint airborne LiDAR. *Remote Sens. Environ.* 87, 171–182.